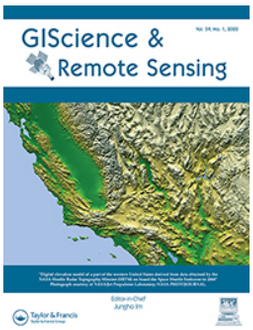

GIScience & Remote Sensing

ISSN: (Print) (Online) Journal homepage: www.tandfonline.com/journals/tgrs20

An evaluation of PlanetScope images for 3D reconstruction and change detection – experimental validations with case studies

Debao Huang, Yang Tang & Rongjun Qin

To cite this article: Debao Huang, Yang Tang & Rongjun Qin (2022) An evaluation of PlanetScope images for 3D reconstruction and change detection – experimental validations with case studies, GIScience & Remote Sensing, 59:1, 744-761, DOI: 10.1080/15481603.2022.2060595

To link to this article: https://doi.org/10.1080/15481603.2022.2060595

Published online: 06 Apr 2022.

GISCIENCE & REMOTE SENSING
2022, VOL. 59, NO. 1, 744–761
https://doi.org/10.1080/15481603.2022.2060595

Taylor & Francis
Taylor & Francis Group

An evaluation of PlanetScope images for 3D reconstruction and change detection – experimental validations with case studies

Debao Huang[a,c], Yang Tang[a,b] and Rongjun Qin[a,b,c,d]

[a]Geospatial Data Analytics Lab, The Ohio State University, Columbus, OH, USA; [b]Department of Civil, Environmental and Geodetic Engineering, The Ohio State University, Columbus, OH, USA; [c]Department of Electrical and Computer Engineering, the Ohio State University, Columbus, OH, USA; [d]Translational Data Analytics Institute, The Ohio State University, Columbus, OH, USA

ABSTRACT

The PlanetScope satellite constellation has over 130 Dove satellites running 24/7, which collect weekly and even daily images globally at 3–5 m resolution. It has global data coverage and high temporal resolution, which constitute the most attractive features for medium-resolution 3D reconstruction and change detection in remote sensing applications. One shortfall of the PlanetScope images is that they are often captured at very small off-nadir angles to minimize relief differences for 2D time-series image analysis, which is not intended for classic stereo 3D reconstruction due to the very small base-to-height ratios of stereo pairs. However, considering the abundant PlanetScope images, the multi-view stereo 3D reconstruction approach leveraging a large number of images may drive the possibility of achieving more accurate 3D reconstruction, and consequently, 3D change detection on a global scale. In this paper, a multi-view stereo 3D reconstruction pipeline was adopted to comprehensively evaluate the 3D potential of PlanetScope images by performing accuracy analysis for both 3D reconstruction and change detection in semi-randomly selected regions with ground truth data. Three case studies using the PlanetScope images were performed: (1) a case study on multi-view stereo 3D reconstruction, (2) a case study on 3D change detection of buildings and trees, and (3) a case study on volumetric estimation for natural disaster monitoring. Our experiments showed that the PlanetScope images provided sufficient coverage for multi-view stereo 3D reconstruction given an area of interest. It could achieve a reasonably acceptable accuracy with root-mean-square errors of 4–6 m in our test regions and detect significant 3D changes. The capability of estimating the volumetric changes was also evaluated for the recent avalanche in Chamoli, India, and the estimated volume favorably matched the results from existing studies using data with higher resolution.

ARTICLE HISTORY
Received 27 August 2021
Accepted 26 March 2022

KEYWORDS
Multi-view stereo 3D reconstruction; accuracy assessment; 3D change detection

1. Introduction

The PlanetScope satellite constellation has over 130 satellites running 24/7, which collect weekly and even daily images globally at 3–5 m resolution (or ground sampling distance – GSD). This has enabled a great potential for 2D remote sensing applications on a global scale. For example, PlanetScope images have been used for deforestation detection (Francini et al. 2020; Caballero Espejo et al. 2018; Finer et al. 2018), crop health analysis (Sagan et al. 2021; Breunig et al. 2020; Kokhan and Vostokov 2020), and wildfire monitoring (Chung, Han, and Kim 2020; Kim, Jung, and Kim 2019).

The richness of the PlanetScope datasets has recently brought up the possibility of using them to perform 3D photogrammetric reconstruction and generate global-scale digital surface models (DSM) (Ghuffar 2018). To date, high-resolution DSMs (Loghin, Otepka-Schremmer, and Pfeifer 2020; Wang et al. 2019) are still expensive to acquire, and their global coverage and temporal resolution are inadequate. Other sources such as Sentinel-1 synthetic aperture radar (SAR) sensors may supply data for highly accurate deformation analysis through interferometric SAR approaches (Amitrano et al. 2014; Shi, Yang, and Liu 2011; Wright, Parsons, and Zhong 2004). However, 3D data from these sources generally lack spatial and temporal resolution (Capaldo et al. 2012). The PlanetScope satellites are originally designed to collect well-registered 2D images purposely at very small off-nadir angles to minimize the impact of relief differences on image registration. Although these images are not intended for 3D reconstruction due to the small base-to-height (*B*/*H*) ratios of potential stereo pairs, researchers have attempted to use a large number of stereo pairs to produce reasonably accurate DSMs (d'Angelo and Reinartz 2021; Aati and Avouac 2020;

CONTACT Rongjun Qin qin.324@osu.edu

Ghuffar 2018). Ghuffar (2018) performed DSM generation from the PlanetScope images in a multi-view stereo (MVS) configuration, in which a semi-global matching (SGM) algorithm was used for stereo matching, followed by a median filter-based DSM fusion. The reported results achieved a normalized median absolute deviation (NMAD) varying from 3.9 to 8.9 m, while no root-mean-square errors (RMSE) were reported. d'Angelo and Reinartz (2021) used a similar approach to fuse DSMs generated from multiple stereo pairs with convergence angles larger than 6° on a test region in Terrassa, Spain, where the light detection and ranging (LiDAR) data (Reinartz et al. 2010) is available as ground truth for accuracy evaluation. The results of fusing DSMs generated from over 100 stereo pairs were reported to achieve an RMSE of 5.5 m for the Teressa region. Their visual results suggested that the DSMs from the PlanetScope images were not able to reconstruct urban structures. Aati and Avouac (2020) performed a study to assess the potential of the PlanetScope images for 3D reconstruction and change detection on a glacial site. The evaluation of 3D reconstruction was performed by comparing the reconstructed digital elevation models (DEM) with the Shuttle Radar Topography Mission (SRTM) DEMs (Farr et al. 2007) and a DEM generated from higher-resolution GeoEye-1 (GE-1) and WorldView-2 (WV-2) stereo images, which reported an NMAD of 7–12 m. Their works also reported that the results of 3D change detection were consistent with the results obtained from Advanced Spaceborne Thermal Emission and Reflection Radiometer (ASTER) and SRTM DEMs. However, detailed accuracy analysis between the PlanetScope DEMs and more accurate reference data (such as LiDAR-derived DEMs) was not performed.

In summary, the existing works (d'Angelo and Reinartz 2021; Aati and Avouac 2020; Ghuffar 2018) acknowledged that the PlanetScope images had the possibility of generating DSMs at the landscape level and indicated that these DSMs had better resolution than the available SRTM data. However, they did not provide a thorough study of this data source and its potential for serving applications that demand 3D data for the following reasons. First, existing evaluations were mostly performed on single sites, yet lacked the confidence to understand the 3D results of the PlanetScope images at generally any area of interest (AOI). Second, using a large number of selected pairs (*i.e.* all with convergence angles larger than 6°) from the PlanetScope images may create over-smoothed DSMs (d'Angelo and Reinartz 2021). As indicated by Qin (2017), simply increasing the number of stereo pairs (from any data source) for reconstruction may not necessarily improve the reconstruction results; thus, it is worth exploring further to understand the achievable 3D reconstruction accuracy from the PlanetScope images. Third, the PlanetScope images with high temporal resolution may enable not only 2D but also 3D change detection (Qin, Tian, and Reinartz 2016; Qin 2014) because monthly or quarterly collected images may be sufficient to reconstruct time-series DSMs for 3D change detection. There existed 3D change detection studies on objects such as buildings (Stal et al. 2013; Murakami et al. 1999), glaciers (Aati and Avouac 2020; Podgórski et al. 2019), and forests (Tian et al. 2013; Xiaowei et al. 2006). However, these studies used data from other well-investigated sources, and few of them reported the possibility of using the PlanetScope images. Hence, it is worth exploring such a capability for the PlanetScope images. In this paper, we evaluated these potentials and informed the community of the usability of PlanetScope images by answering the following three questions:

(1) Given any AOI, are there sufficient PlanetScope images for performing high-quality 3D reconstruction, and how accurate are the DSMs derived from the PlanetScope images?
(2) Do these DSMs have sufficient temporal resolution to perform accurate 3D change detection? If so, what level of changes can be detected?
(3) Can PlanetScope images be used to analyze the impacts of natural disasters anywhere on earth? If so, how accurate is it?

To answer these, we devised three case studies using the PlanetScope images and their 3D reconstruction results: 1) an accuracy analysis study on two sites where LiDAR datasets are available, *i.e.* the International Society for Photogrammetry and Remote Sensing (ISPRS) benchmark datasets (Reinartz et al. 2010); 2) a 3D change detection study specifically on trees, which was noted as a challenging task in previous studies such as Kempf et al.'s (2021), 3) a case study on evaluating the volumetric estimation of the recent avalanche in Chamoli, India. It should be noted that these study areas were selected semi-randomly, only based on the availability of ground truth data, and the source images were collected from the Planet data archives (Planet Team). Therefore, we expected that the availability and possible stereo

configurations analyzed on our test sites should be valid for any other AOIs. We collected on average 10–15 images for each site, and for the second and third case studies, two temporal datasets for each site were collected to perform 3D change detection. We adopted an MVS 3D reconstruction pipeline as introduced by Qin (2017) to perform the 3D reconstruction for these sites. Accuracies of 3D reconstruction and change detection were evaluated based on the available LiDAR data.

The remainder of this paper is organized as follows: Section 2 introduces our evaluation methodologies, including data collection and the base method for 3D reconstruction and 3D change detection; Section 3 shows the results and our answers to the above mentioned three research questions; Section 4 describes our result analysis; Section 5 concludes this paper with our discussion on the potential usability of the PlanetScope images as a 3D remote sensing asset.

2. Methodology

2.1. Experiment setup

2.1.1. Test regions

To perform our proposed studies for (1) 3D reconstruction, (2) 3D change detection, and (3) volumetric estimation in post-disaster assessment, we selected five AOIs where the PlanetScope data were collected as shown in Figure 1 and Table 1. These regions were selected to cover various types of landscapes. In case study 1, we included one urban area and one rural area for 3D reconstruction, being Terrassa and La Mola in Catalonia, Spain. The Terrassa site contains dense buildings, large man-made architectures, and hilly areas with trees. The La Mola site contains mountainous areas. The ISPRS benchmark datasets are available for evaluation on these two sites.

For case study 2 on 3D change detection, we included one urban area and one forested area, located in Allentown in Pennsylvania, U.S.A., and Americus in Georgia, U.S.A., respectively. Different types of changes can be found in these two areas. In Allentown, the objects of focus are buildings near the Lehigh River subject to demolition (Figure 8). LiDAR data are available before and after the demolition event, which were surveyed in 2016 and 2019. The dimension of the building is approximately 160 m × 30 m × 18 m for building length/width/height, highlighted within the circled region in Figure 8a. In Americus, there was a logging event in a forested area (Figure 9) from December 2019 to January 2020. The size of the forested area is approximately 1000 m × 700 m, and the average height of the trees is roughly 20 m. LiDAR data are available for both pre- and post-event periods, which were surveyed in 2016–2017 and 2020.

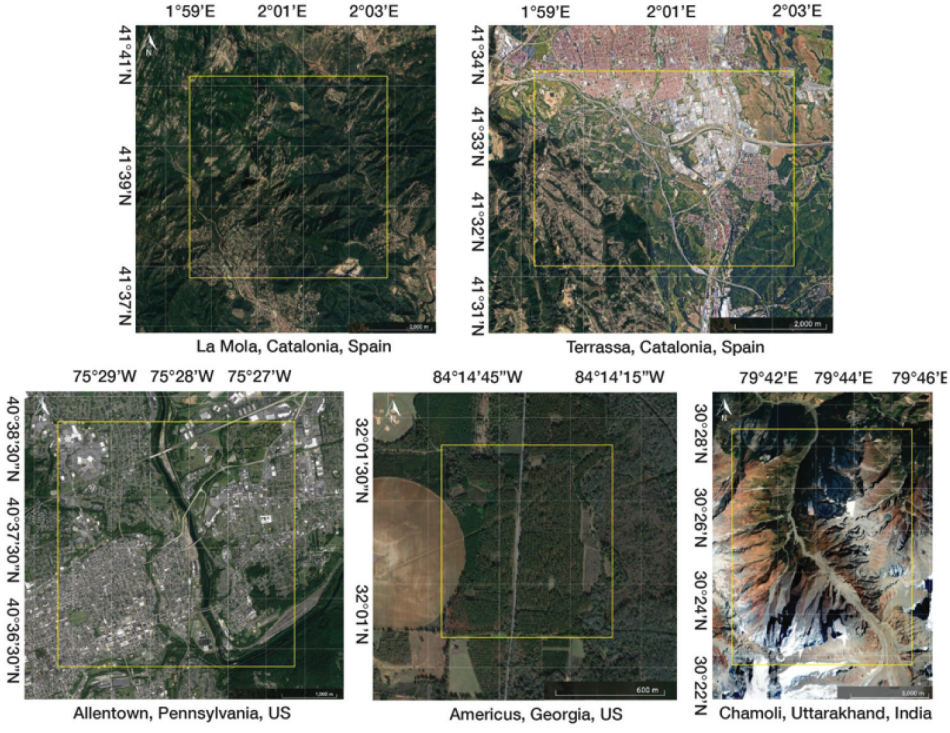

Figure 1. Locations of the five test regions are shown in yellow outlines.

Table 1. Descriptions of the five test areas for 3D reconstruction, 3D change detection, and post-disaster assessment.

Region	Type	Area (km^2)	Elevation (m)	Study purpose	Data collection window (yymmdd)	Reference
La Mola, Catalonia, Spain	Mountainous	29.38	333–1094	3D reconstruction	200801 – 210424	LiDAR
Terrassa, Catalonia, Spain	Urban, hilly	16.96	149–396	3D reconstruction	210211 – 210418	LiDAR
Allentown, Pennsylvania, United States	Urban	17.69	69–239	3D change detection	141103 – 160620 190326 – 190922	LiDAR
Americus, Georgia, United States	Forested	0.71	95–142	3D change detection	190322 – 191130 200105 – 200402	LiDAR
Chamoli, Uttarakhand, India	Mountainous, glacial	42.09	3101–5790	Post-disaster assessment	201213 – 210206 210207 – 210226	Results from existing studies (Martha et al. 2021; Pratima et al. 2021; Shugar et al. 2021)

For case study 3 on post-disaster assessment, we included a glacial area in Chamoli, India, where the Uttarakhand flood happened on 02/07/2021, killing at least 72 people and leading to massive damages in the Chamoli district. The flood was caused by an avalanche from the Ronti peak, which created significant topological changes. Although LiDAR data is not available, there happened to be existing works (Martha et al. 2021; Pratima et al. 2021; Shugar et al. 2021) that used satellite data with higher resolution to estimate the volume of rock and ice. For example, Martha et al. (2021) used stereoscopic CartoSat-1 data collected in November 2018 and Pleiades-1B data collected in February 2021 to generate DEMs for pre- and post-disaster periods. Therefore, we used these results as references for our study.

2.1.2. Data collection

Given an AOI, we collected the PlanetScope images from the Planet data archives by considering three criteria: (1) the images need to be cloud-free, (2) the images should cover 100% of the AOI, and (3) images with systematic temporally varying artifacts such as snow or high reflection of water surface should not be considered. We gave higher priority to images with large off-nadir angles because such images would have a higher chance to yield stereo pairs with large convergence angles. The data acquisition time frame was kept as short as possible to avoid temporal changes, while at the same time allowing a sufficient number of images to be collected. However, for specific events (*i.e.* avalanches), the selection of images was often limited to a narrow time frame. Hence, the number of qualified images might be insufficient. In this scenario, we included images with smaller off-nadir angles to allow a sufficient number of images to be collected.

2.2. The 3D reconstruction pipeline

Although 3D reconstruction from bi-stereo satellite images was standard practice, the use of multi-view satellite images was only getting popularized in recent years due to the increasing availability of the source satellite data (d'Angelo and Reinartz 2021; Loghin, Otepka-Schremmer, and Pfeifer 2020; Ghuffar 2018; Qin 2017). Existing works showed that utilizing a large number of satellite images for 3D reconstruction could be extremely useful to generate high-quality DSMs. For example, the prior work (Qin 2019a) verified that the MVS 3D reconstruction using very high resolution (VHR) images (with a GSD of 0.3–2 m) generated DSMs with vertical accuracy of 1 m. The MVS paradigm was used in their work, which performed pairwise stereo reconstruction followed by a depth fusion process (Bhushan et al. 2021; Qin 2019b, 2017). This MVS paradigm held the advantages of being more flexible and easier for implementation.

In our evaluation, we used the same MVS 3D reconstruction pipeline used in Qin (2017), and the workflow is shown in Figure 2. Given a set of images, we took every possible pair for reconstruction. A pairwise bias compensation (Fraser and Hanley 2003) using tie points was performed to achieve relative orientation, followed by a dense image matching using a hierarchical SGM algorithm (Qin 2016; Hirschmuller 2007). Those DSMs produced by pairs with large convergence angles (here we used 8° as a large convergence

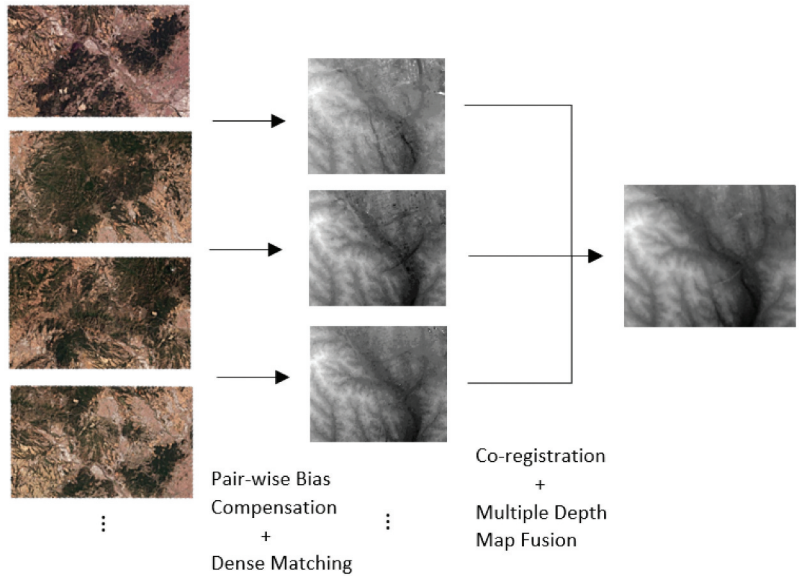

Figure 2. The MVS 3D reconstruction pipeline used for evaluating the planetscope images. explanations of this pipeline are in the texts.

angle for the PlanetScope data) were then registered, and a multiple depth map fusion was performed to yield the fused DSM. The fusion algorithm considered both spatial consistency and boundary preservation: instead of using a median filter that computed the median value of the height at each pixel, a window was defined based on a weighted Gaussian kernel using the spatial and color proximities to the centric pixel. The height values of those pixels within the window were used to perform weight median filtering (Qin 2017). The readers may refer to the details of this pipeline in (Qin 2019a, 2017).

2.3. Method for 3D change detection and volumetric change estimation

We performed the 3D change detection by considering only the geometric differences (*i.e.* height differences) of two DSMs generated by the datasets collected from two different periods. The generated DSMs of the pre- and post-event were respectively registered to the LiDAR reference DSMs of the pre- and post-event using a least-squares surface matching method (Gruen and Akca 2005). The height differences of the reconstructed DSMs were then compared with the height differences of the LiDAR DSMs, which evaluated the ability of the PlanetScope images to perform geometry-based change detection. The height difference and the actual area of each grid in DSM were aggregated to estimate the volumetric changes.

3. Results

3.1. Data availability

To understand the availability of the PlanetScope images for each AOI and their geometry configurations (*i.e.* the off-nadir angles), we drew the histogram of the available images (1000+ images per site) and their off-nadir angles for these five sites, which were collected between 01/01/2016 and 06/01/2021 (shown in Figure 3). Except for a minor difference in the Chamoli region, almost all the test regions showed similar distributions of their off-nadir angles: approximately 40% of these images had nearly 0° off-nadir angles, and only 10–15% of the images had off-nadir angles equal to or larger than 5°. Therefore, the convergence angles of possible pairs, which considered the azimuth angle differences as well, may range from 0° to 10° and few could be beyond 10°.

In our case study 1, two test regions, La Mola and Terrassa, were selected to analyze the accuracy of MVS 3D reconstruction. A total of 10 PlanetScope images were acquired for each site. These images were acquired within 2–8 months, and detailed information of the selected images is listed in Table 2. The selected 10 images constituted 45 possible stereo pairs with various convergence angles for each site. Figure 4 shows the distributions of convergence angles of the stereo pairs, and it could be seen that the convergence angles of most of the pairs were very small (smaller than 3°), while there were still a good number (ca. 30%) of stereo

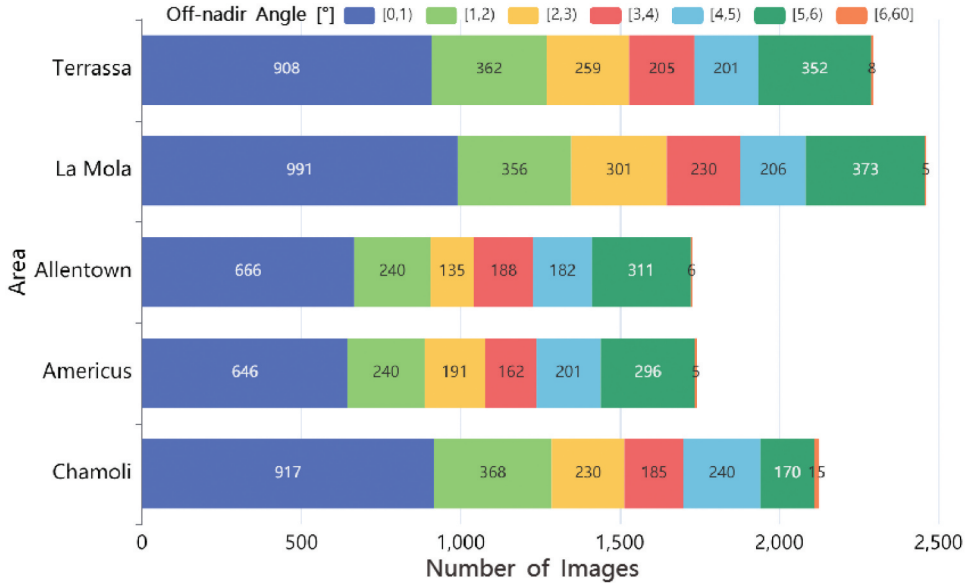

Figure 3. Distributions of off-nadir angles of the planetScope images for the five test regions between 01/01/2016 and 06/01/2021.

pairs with convergence angles larger than 8°, and some reached 13°. We used a threshold of 8° to filter stereo pairs to retain approximately 30% of the images. As mentioned before, these observations about the convergence angles were representative in most of the cases, being that the off-nadir angles of the PlanetScope images were mostly smaller than 6°, and the achievable largest convergence angle was about 13°. Detailed results and evaluation of this case study are introduced in Section 3.2.

In our case study 2, two test regions, Allentown and Americus, were selected to assess the ability of PlanetScope images to perform 3D change detection of ground objects. Table 2 lists the statistics of the collected data for both test regions, showing that the number of collected images variably ranged from 8 to 15. The pre-event images generally spanned a longer period than the post-event images. Especially for Allentown, the dates of the collected images spanned 2 years (2014–2016), which was primarily due to the lack of satellites in the early years (before 2018). This was also reflected by the poor convergence angles of the constructed stereo pairs as shown in Figure 4. Thus, it was expected that the reconstructed DSM could be poor. For images collected after 2018, the temporal resolution got increasingly higher as more satellites were launched. Therefore, it required a shorter period to collect the same number of images. Figure 4 shows the distributions of the convergence angles of stereo pairs constructed from the collected images. Detailed results and evaluation of this case study are introduced in Section 3.3.

In our case study 3, the last test region, Chamoli, was selected to assess the ability of PlanetScope images to derive accurate volumetric statistics for post-disaster assessment. A total of 11 PlanetScope images were acquired for each of the pre- and post-disaster periods, within two months before the disaster and within three weeks after the disaster (statistics are shown in Table 2). This yielded in total 55 stereo pairs for each period, whose histogram of convergence angles is shown in Figure 4. Like other sites, approximately 30% of the stereo pairs had convergence angles larger or equal to 8°, indicating their potential for generating reasonably good geometry from these images. Detailed results and evaluation of this case study are introduced in Section 3.4.

The data availability statistics of the five sites answered our first research question in Section 1: in general, for each site, the number of available images was more than 1,000 within the time frame between 2016 and 2021, with the higher temporal resolution for data collected after 2018 due to the increased number of satellites in the constellation. Although it was possible to collect sufficient data before 2018 with a certain

Table 2. Data acquisition information of the five test sites.

Region	La Mola (10 images)									
Acquisition date (yymmdd)	200801	201006	201115	201118	210211	210310	210321	210323	210330	210424
Off-nadir angle (°)	0.008	5.034	5.048	4.987	5.033	5.149	5.033	4.988	5.070	2.950
Region	Terrassa (10 images)									
Acquisition date (yymmdd)	210211	210310	210321	210322	210323	210325	210329	210330	210403	210418
Off-nadir angle (°)	5.038	5.196	5.031	5.034	4.976	4.994	5.037	5.072	4.975	4.926
Region	Allentown, pre-event (8 images)									
Acquisition date (yymmdd)	141103	141103	151011	160222	160302	160417	160420	160620		
Off-nadir angle (°)	2.954	2.852	3.179	1.860	4.344	1.738	2.497	1.125		
Region	Allentown, post-event (8 images)									
Acquisition date (yymmdd)	190326	190502	190603	190628	190917	190919	190921	190922		
Off-nadir angle (°)	5.015	5.015	5.376	4.992	5.019	5.014	4.997	4.998		
Region	Americus, pre-event (15 images)									
Acquisition date (yymmdd)	190322	190328	190415	190727	190829	190905	190920	190922		
	191002	191028	191102	191109	191117	191118	191130			
Off-nadir angle (°)	5.206	5.010	4.982	4.994	5.030	5.006	4.991	4.991		
	4.997	4.995	5.068	5.014	4.972	4.968	5.040			
Region	Americus, post-event (11 images)									
Acquisition date (yymmdd)	200105	200120	200202	200214	200215	200222	200227	200229	200301	200306	200402
Off-nadir angle (°)	5.054	5.379	3.991	3.765	4.956	5.064	4.979	4.980	3.039	2.987	5.042
Region	Chamoli, pre-disaster (11 images)									
Acquisition date (yymmdd)	201213	201214	201215	210110	210110	210111	210112	210205	210205	210206	210206
Off-nadir angle (°)	4.211	2.031	4.987	4.979	4.978	0.883	3.965	0.115	4.971	4.966	3.986
Region	Chamoli, post-disaster (11 images)									
Acquisition date (yymmdd)	210207	210208	210209	210209	210209	210210	210213	210214	210216	210222	210226
Off-nadir angle (°)	4.984	4.937	3.928	0.376	0.39	4.994	2.916	4.019	2.982	1.912	0.373

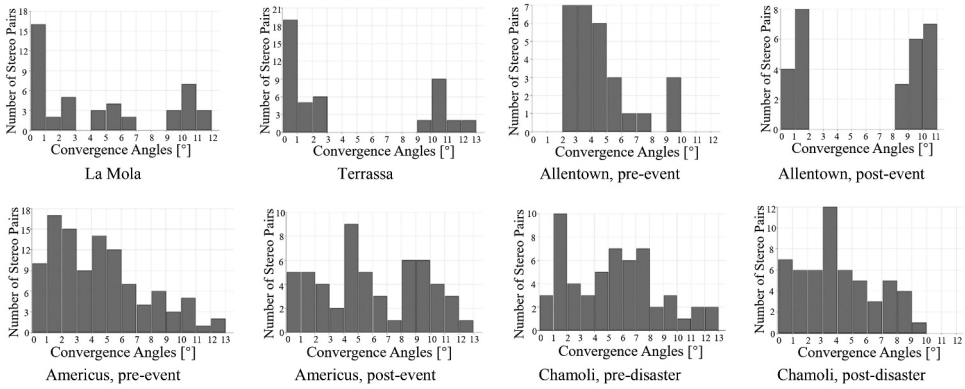

Figure 4. Distribution of convergence angles for the five test sites.

effort, data after 2018 were much more available and more likely to yield sufficient stereo pairs (more than 9) with convergence angles larger than 8° for MVS 3D reconstruction. The availability in terms of coverage and temporal resolution of the PlanetScope images exceeded most of the other competing sources for MVS 3D reconstruction given an arbitrary AOI on earth.

3.2. Results of 3D reconstruction – case study 1

3.2.1. Qualitative and quantitative assessment of the reconstructed DSM

Figure 5 shows the MVS reconstructed results with comparison to LiDAR-derived DSMs. For quantitative comparison, the LiDAR DSMs were resampled at the same spatial resolution (4 m) of reconstructed DSMs. We could observe from the visual results that the main topography of the landscape was well reconstructed, and it showed some over-smoothed effects at the contours of ridges and valleys, which was reasonable considering its spatial resolution of 4 m. The Terrassa site consisted of challenging landscapes with mixed urban and hilly areas. A similar study in this region was performed by d'Angelo and Reinartz (2021), who used hundreds of stereo pairs to reconstruct the topography of the landscape. Their resulting DSMs were over-smoothed and did not succeed in reconstructing any building objects. However, since we used highly selected stereo pairs with large convergence angles in our experiment, we were able to observe a few large man-made architectures (larger than 100 m × 100 m) in the reconstructed DSM (third row of Figure 5), although most of the smaller buildings were not reconstructed.

We further performed a quantitative study to evaluate the accuracy of the reconstructed DSM, whose error distributions compared to the LiDAR DSMs are shown in Figure 6. The reconstructed DSMs were registered to the LiDAR DSMs using a least-squares surface matching (Gruen and Akca 2005) method, with the sigma-naught of 0.19 m and 0.18 m, respectively, for the La Mola and Terrassa sites. We observed that the RMSE of the La Mola site was 43% worse than that of the Terrassa site, and the residual maps in Figure 6a shows that this was largely attributed to the reconstruction errors at sharp ridges of the La Mola site, where high relief differences introduced large vertical errors. On the contrary, the topography of Terrassa was generally smoother, which was more favored by the reconstruction given the relatively low spatial resolution of the image. Larger errors were only found on the sparsely distributed tall buildings (circled in Figure 6b) and sharp ridges. This observation was further validated through the correlation scatter plots in Figure 6, which draws the elevation of the reconstructed DSMs and the reference LiDAR DSMs for both sites. The statistics of the La Mola site showed a thicker band reflecting higher uncertainty than that of the Terrassa site, further evidencing that the reconstructed DSM of Terrassa generally contained a smoother landscape topography.

The experiments of the La Mola and Terrassa sites answered our first research question in Section 1 about the accuracy of 3D reconstruction for the PlanetScope images. In summary, an RMSE of 4–6 m of the reconstructed DSM for these sites reflected reasonable

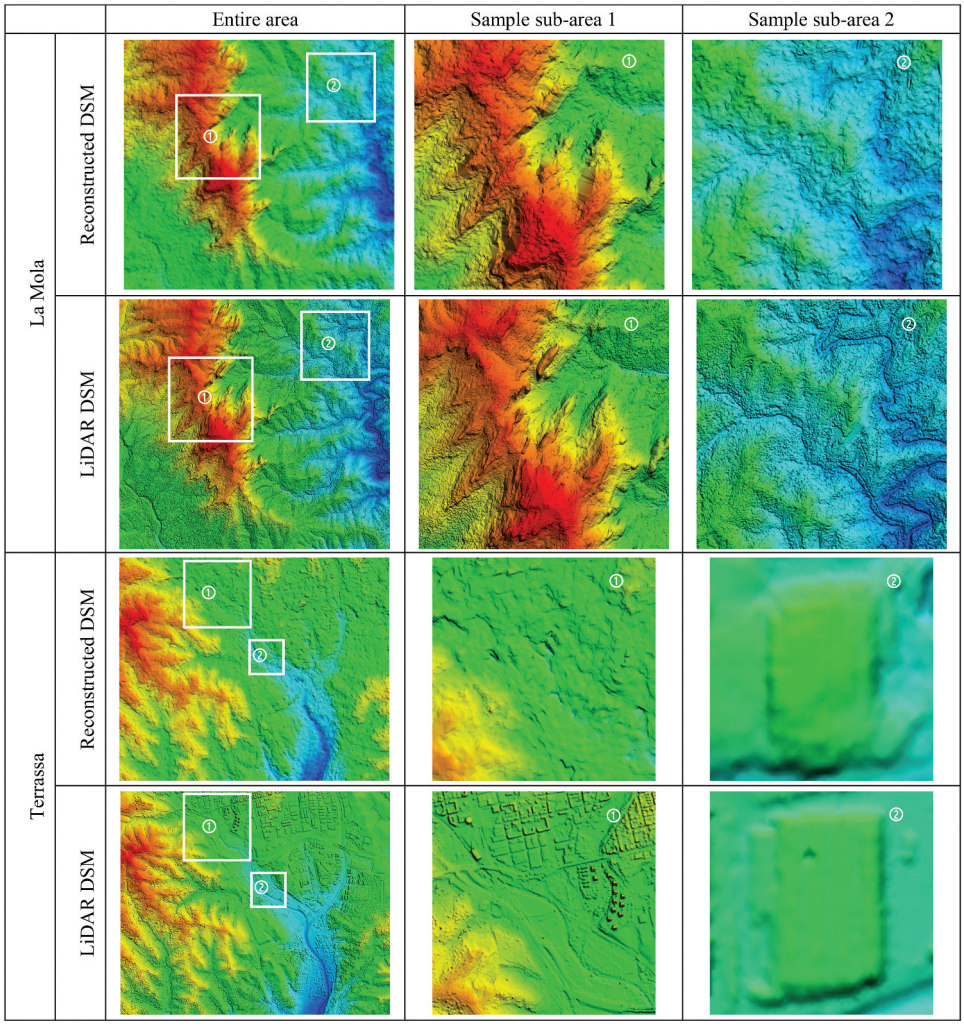

Figure 5. A visual comparison between the planetscope reconstructed DSMs and LiDAR DSMs of the entire areas and two marked sub-areas in la mola and terrassa sites. it should be noted that the reconstructed DSM of the terrassa site did reconstruct a large building (third row, last column).

reconstruction accuracy. Considering that the GSD of the PlanetScope images is only 3–5 m, the RMSE of the reconstructed DSM is equivalent to 1–2 pixels in terms of the pixel size. It was also surprising that the reconstruction in the Terrassa region did pick up some large man-made buildings in our study, as opposed to the conclusion of the previous studies using PlanetScope images (d'Angelo and Reinartz 2021). Part of the reason was that their study used hundreds of pairs that may smooth out these objects, while our method used highly selective stereo pairs that could obtain sharper DSMs. Thus, with its global data coverage, we considered it a reasonable alternative for the basic terrain layer such as the SRTM dataset (Farr et al. 2007).

3.2.2. Relationship between the reconstruction accuracy and The number of stereo pairs

In the experiments, the number of images used for the DSM reconstruction also determined the reconstruction accuracy. Therefore, we investigated the relationship between the reconstruction accuracy and the number of stereo pairs for the two tested sites, as shown in Figure 7. To make the investigation tractable, we only used stereo pairs with convergence angles larger than 8°. Figure 7 shows that the RMSE generally improved as more stereo pairs were considered. Fluctuations were observed in the trend curve when relatively fewer pairs were used (*i.e.* smaller than five), and this could be explained that with fewer DSMs, poor

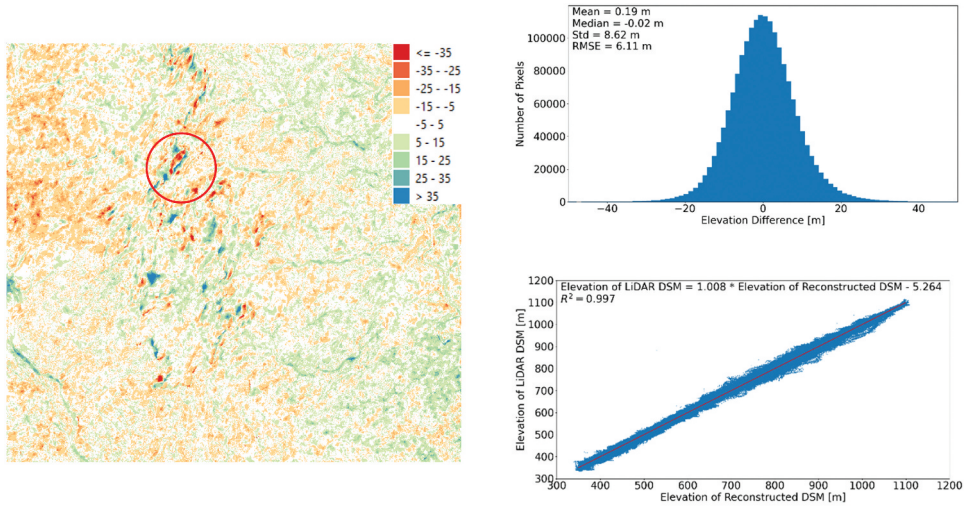

(a) La Mola

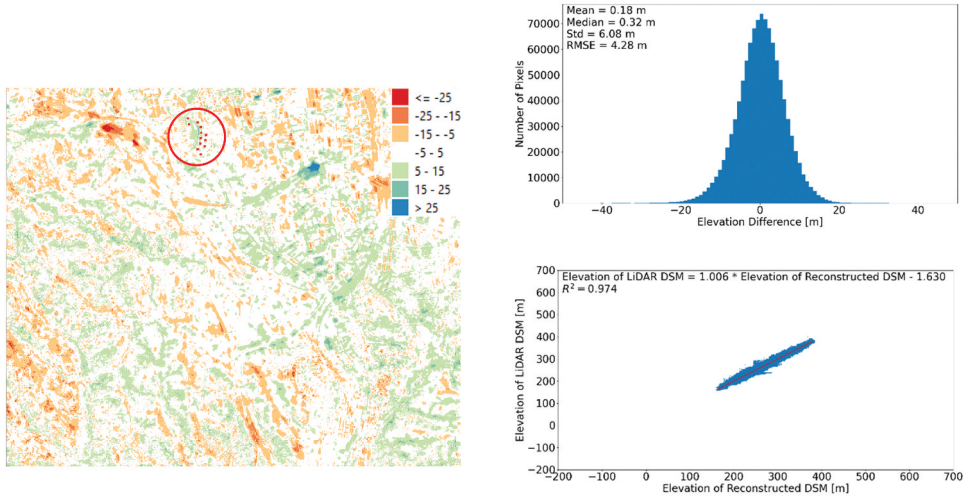

(b) Terrassa

Figure 6. Elevation differences between LiDAR DSMs and planetscope reconstructed DSMs for the la mola and terrassa sites. left: error distribution maps. right: error distributions and statistics. circled regions in the error maps highlight where large errors occur (explanations are in the text).

DSMs out of them might have relatively larger impacts. When the number went above six, it showed a more stable trend with reducing RMSE. For the La Mola and Terrassa sites, we observed that eight stereo pairs and more provided reasonably good results, achieving about 30% of accuracy improvement on a single pair.

3.3. Results of 3D change detection – case study 2

Allentown site

The 3D change detection results of the Allentown site are shown in Figure 8. As mentioned in Section 2.1.1, LiDAR reference DSMs are available for accuracy evaluation. Thus, we computed the RMSE of the reconstructed DSMs for both the pre- and post-event periods as shown in Table 3. The images in the pre-event period were mostly collected before 2018, at a time when the number of satellites of this constellation and the image quality were not as good as the recent satellites (after 2018). This resulted in a fewer number of desirable stereo pairs, which only reached an RMSE of 15 m based on our evaluation in Section 2.2. Although the accuracy of the post-event DSM reached approximately an RMSE of 4–5 m, it was expected that the poor quality of pre-event DSM may significantly affect the results of change detection.

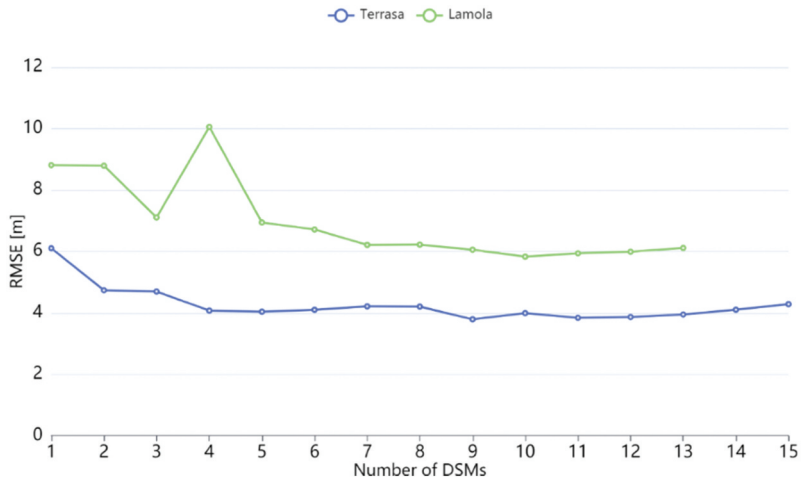

Figure 7. Relationship between RMSE and number of DSMs used for fusion in la mola and terrassa sites.

Table 3. Error statistics for the Allentown and Americus sites.

Site	Period	Mean (m)	Median (m)	Standard Deviation (m)	RMSE (m)
Allentown	Pre-event	−0.44	−1.73	19.46	15.76
	Post-event	−0.05	0.02	7.03	4.87
Americus	Pre-event	1.92	0.32	6.54	4.66
	Post-event	−0.93	−0.52	6.85	4.88

Figure 8 depicts the visual results of 3D change detection in the Allentown site. As expected, due to the poor reconstruction quality of the pre-event DSM, the profiles of the pre- and post-event DSMs did not reflect changes as reflected by the reference LiDAR DSMs. As shown in Figure 8d and Figure 8e, the profiles of pre- and post-event LiDAR DSMs showed a clear height difference indicating a building demolition event, while the PlanetScope reconstrued DSMs failed to capture the changes. In addition to the inadequate data acquired in early years, which caused the poor reconstruction of pre-event DSM, the failure was attributed to the relatively low resolution of PlanetScope images, since a building with a physical dimension of 160 m × 30 m (40 × 7.5 in pixels, equivalently an area of 300 pixels on the image) was too small for typical change detection algorithms. According to Qin (2014), changes in an area smaller than 1,600 pixels (40 × 40) could hardly be detected in 3D data.

Americus site

The 3D change detection results of the Americus site are shown in Figure 9. At this site, a logging event occurred in an area of 1000 m × 700 m (equivalently 250 × 175 = 43,750 pixels), indicated in the circled region of Figure 9. Table 3 lists the accuracy of both the pre- and post-event PlanetScope reconstructed DSMs, which achieved an RMSE in the range of 4–5 m. According to our case study 1, this RMSE indicated that the DSMs were reasonably well reconstructed. The visual results in Figure 9 (first two rows) showed that the reconstructed DSMs not only reflected the height differences well, but were also consistent with what the LiDAR DSMs captured. Furthermore, the side-by-side DSM profiles (the third row of Figure 9) provided a zoom-in comparison to depict the consistent observations between the PlanetScope DSMs and the LiDAR DSMs of the pre- and post-event. To investigate the error distributions of the change detection, we compared the height differences produced by PlanetScope reconstructed DSMs and LiDAR DSMs, respectively, as shown in Figure 10. To be precise, Figure 10a draws the differences of the PlanetScope DSM height changes and the LiDAR DSM height changes, showing the error distributions of the change detection. It could be seen that although there were large errors (larger than 10 m) scattered around the test region, the overall RMSE achieved 6.65 m (Figure 10b), and the standard deviation achieved 6.55 m, which was reasonably accurate

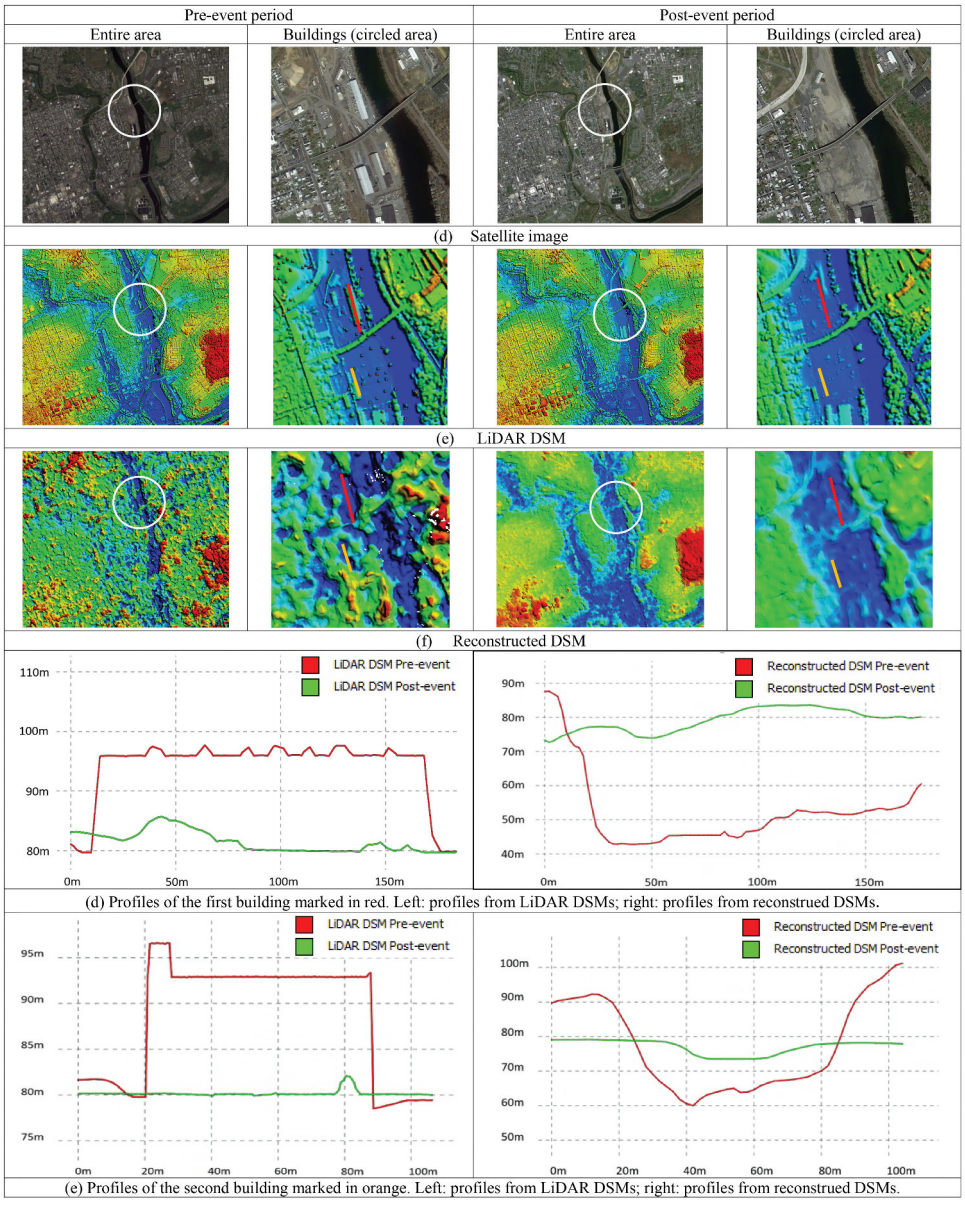

Figure 8. A visual comparison between planetScope reconstructed DSMs and LiDAR DSMs of the entire areas and the demolished buildings in the Americus site. sub-figure (d) and (e) show that the reconstructed DSMs failed to capture the changes and gave conflicting results.

to discern equal and larger height changes. In particular, for this site, since most of the tree patches were significantly higher than the ground (over 20 m), the PlanetScope DSMs indicated positive results in detecting changes resulting from the logging event.

This site had trees and the ground as the only objects in the scene, making it easy to analyze the reconstruction quality for the tree and ground class. Figure 10c draws the height statistics of these two classes in both the pre- and post-event periods for both the PlanetScope DSMs and LiDAR DSMs. It could be seen that the mean value and the height range of the tree pixels in the PlanetScope DSMs were well estimated as compared to those of the LiDAR DSMs. However, the mean value of the ground pixels of the PlanetScope DSMs had a 1-m bias over that of the LiDAR DSM, and the height range was also notably larger. This indicated that the PlanetScope DSMs tended to overestimate the ground pixels variably.

The experiments of the Allentown and Americus sites answered our second research question about the feasibility of 3D change detection asked in Section

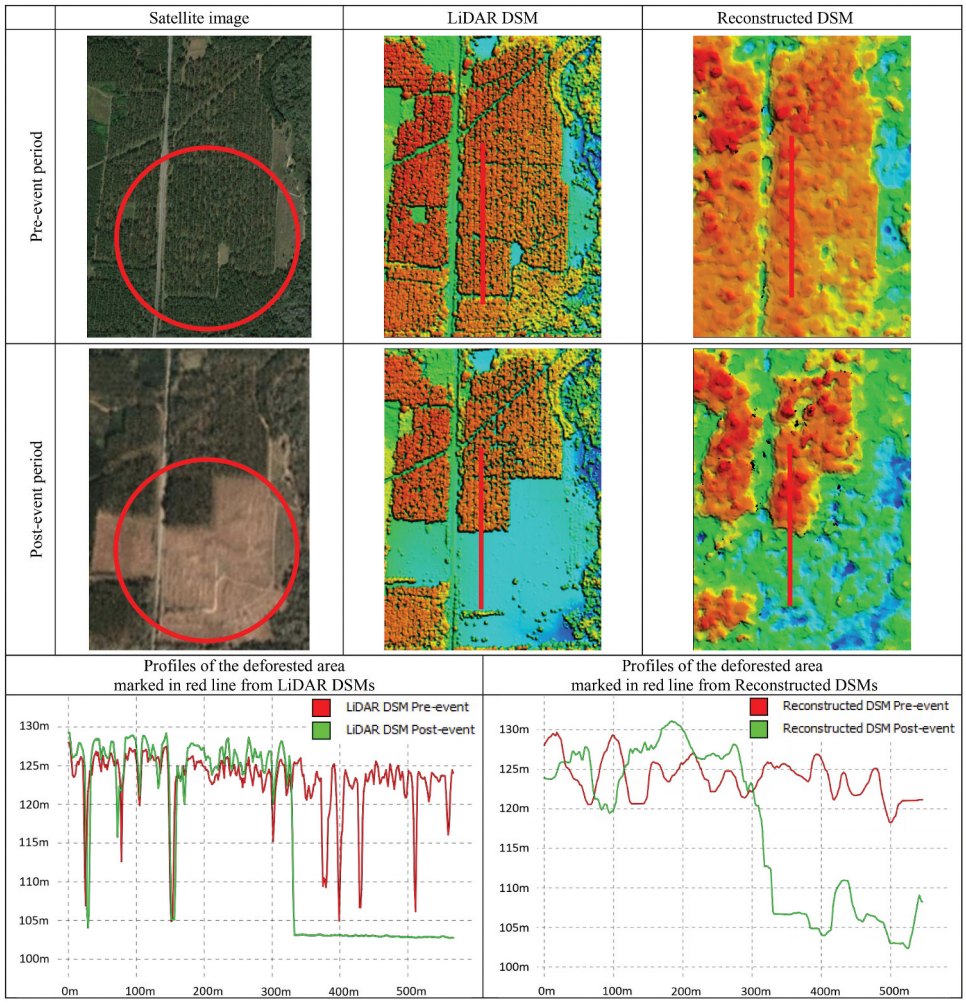

Figure 9. A visual comparison between planetScope reconstructed DSMs and LiDAR DSMs in the Americus site.

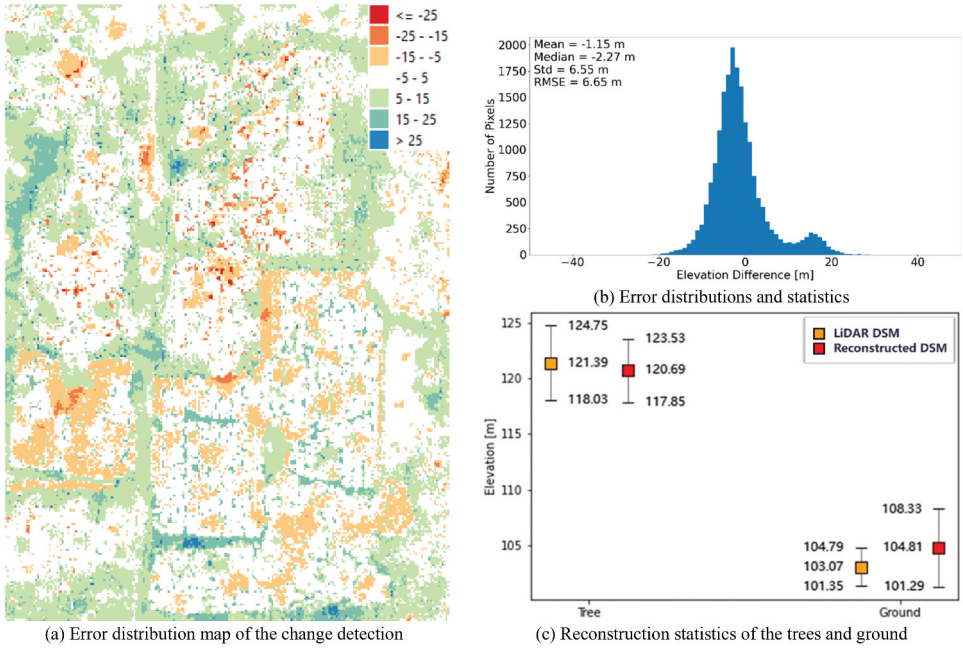

(a) Error distribution map of the change detection

(b) Error distributions and statistics

(c) Reconstruction statistics of the trees and ground

Figure 10. Visual results of 3D change detection for the Americus site to assess the capability of detecting a logging event.

1. We concluded that the PlanetScope DSMs could not be used for detecting changes before 2018 for small areas (*i.e.* smaller than 100 m × 100 m). However, it was possible to use PlanetScope DSMs to detect significant height changes (larger than 8–10 m) with large areas (larger than 1000 m × 700 m) after 2018. In our experiments, we validated that changes in an area of 1000 m × 700 m and a height difference of 20 m were detectable by PlanetScope DSMs.

3.4. Post-disaster assessment – case study 3

The PlanetScope DSMs of the Chamoli test site (details listed in Table 2) before and after the avalanche in February 2021 were used to estimate the volumetric changes. Figure 11 shows the PlanetScope reconstructed DSMs and the change detection results through height difference. First, we observed that the topographies of the entire area were reconstructed well for both periods, as the collected images and the stereo geometric configuration (convergence angles) followed our suggested setups. Second, the elevation differences between the pre- and post-disaster PlanetScope DSMs were significant in the avalanche area (marked in the red triangle of Figure 11c). The changed volume of the avalanche region was computed as 30.36 million cubic meters. Since there was no reference data available, we verified these results by comparing them with conclusions of previous work in (Martha et al. 2021; Pratima et al. 2021; Shugar et al. 2021), which used the Pleiades images with much higher resolution. They reported a volumetric mass change of 27–29.3 million cubic meters, which was close to our estimation.

This case study answered the third research question on the feasibility of the PlanetScope DSM for volumetric estimation of disasters. Based on the

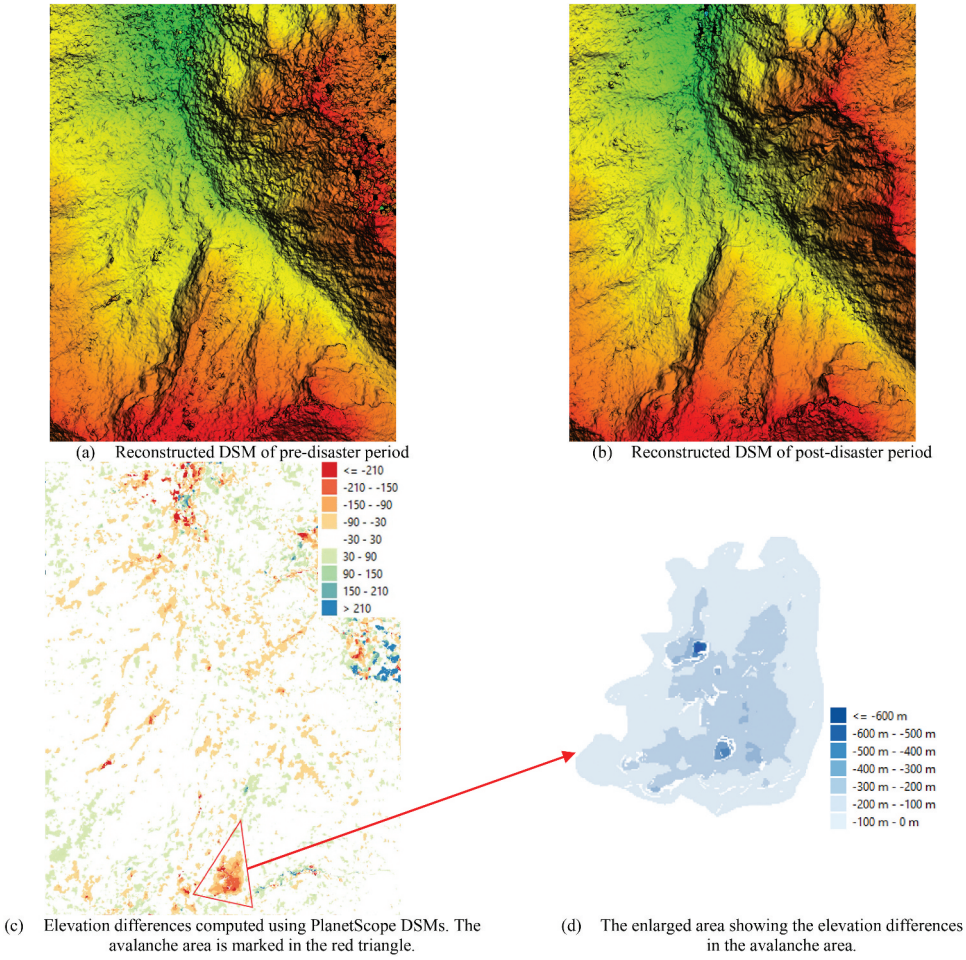

(a) Reconstructed DSM of pre-disaster period

(b) Reconstructed DSM of post-disaster period

(c) Elevation differences computed using PlanetScope DSMs. The avalanche area is marked in the red triangle.

(d) The enlarged area showing the elevation differences in the avalanche area.

Figure 11. Visual results of planetScope reconstructed DSMs and change detection in the chamoli site.

experiment results, we expected that the PlanetScope DSM could be used to evaluate volumetric mass changes for global natural disasters on a similar scale as the avalanche event in Chamoli.

4. Discussion

Our three case studies over the five test sites suggested that although the PlanetScope images were not intended for 3D data acquisition, the reconstructed DSMs following our approach introduced in Section 2.2 served well for 3D reconstruction, 3D change detection, and volumetric estimation. Although only 10–15% of the PlanetScope images had off-nadir angles larger than 5°, we could collect sufficient PlanetScope images in a time frame of 2–8 months since the number of images was ample. This generated sufficient stereo pairs (more than 8 pairs) with convergence angles larger than 8° to produce DSMs with reasonable accuracy (1–2 pixels).

Among the five test sites in our experiments, the reconstruction results of images collected in recent years (after 2018) yielded an RMSE up to 4.2 m compared to the LiDAR reference DSMs. On the one hand, the results confirmed the 3D possibility of the PlanetScope images concluded by previous works (d'Angelo and Reinartz 2021; Ghuffar 2018). On the other hand, we had new findings: previous work suggested that no buildings could be reconstructed by the PlanetScope images, while we found that large building objects (with a size of 100 m × 100 m, equivalently 25 × 25 pixels in the image space) may be reconstructed by using our MVS 3D reconstruction pipeline. Furthermore, we analyzed the impact of stereo pairs with respect to the accuracy of resulting DSM in Section 3.2.2 and found that "eight" seemed to be a magic number that produced the largest accuracy improvement; the DSM generated using 8 highly selective pairs with convergence angles larger than 8° achieved 30% of accuracy improvement on the results generated from a single pair. More pairs may improve marginally further, while an overly large number of pairs, as experimented in (d'Angelo and Reinartz 2021), could produce over-smoothed DSM that missed out large building objects.

Our case study on 3D change detection assessed this potential of PlanetScope images with reference LiDAR data. The investigation of the two testing sites provided three suggestions: first, 3D change detection was better supported for the event that occurred after 2018 because the availability and data quality were significantly better after that time point. Second, the changes were more detectable if the areas of changes are larger than 1000 m × 700 m. Our experiment validated that an area of 1000 m × 700 m is sufficient to yield convincing detection using the PlanetScope images. Third, height changes that were two times greater than the uncertainties of the DSMs were more detectable with confidence. For PlanetScope DSMs with an RMSE of 4–5 m, we expected that the detectable elevation differences should be more than 8–10 m.

Data availability, coverage, and resolution have been the major hurdles for remote sensing-based disaster monitoring. Our experiment in determining the mass loss on the Chamoli site posted an important message to the disaster assessment community: the PlanetScope reconstructed DSMs at 4–5 m spatial resolution could detect significant natural disaster events and estimate the volumetric changes with acceptable accuracy. This seemed to be a plain observation, while considering the global availability of this data at high temporal resolution (monthly or bi-monthly), it created an unprecedented possibility to build a sustainable monitoring program to serve the first responders to confront natural disasters that might happen everywhere and at any time point.

5. Conclusions

This paper assessed the potential of the PlanetScope images for producing 3D results through three case studies to answer corresponding research questions. The results of the three case studies over five test sites suggested the following: first, the PlanetScope images had global coverage with sufficient overlaps and could be used to generate DSMs with an accuracy up to 4–5 m, or approximately 1–2 pixels. It was sufficient to reconstruct landscape topography and occasionally large building architectures. Images collected after 2018 were more likely to constitute more stereo pairs with good convergence angles. Second, the PlanetScope images were available at a level that was possible to build monthly or bi-monthly DSMs to perform 3D change detection. Limited by the resolution, identifying the 3D changes of individual urban objects was not yet practical, while it was possible to detect massive 3D changes of land cover. As experimented in

our case study 2, the temporal DSMs could detect height differences over 10 m with confidence in deforested areas. Furthermore, following our first point, this capability was better supported by images dated after 2018. Third, our experiment on assessing the avalanche event in the Chamoli site showed that the estimated volume of the avalanche (30.36 million cubic meters) using the PlanetScope DSMs, favorably matched the results of existing studies (27–29.3 million cubic meters). On the one hand, the results confirmed the feasibility of the PlanetScope images for volumetric estimation for significant natural disaster events. On the other hand, it opened the opportunity to build a sustainable monitoring program to serve the first responders who demand information of disaster events that may occur anytime and anywhere.

Our evaluation of the PlanetScope data showed its unique capability to capture 3D information for earth observations at high temporal resolution as compared to existing products. Although the 3D potential of the PlanetScope images is limited by the small B/H ratios and the spatial resolution, the accuracy can be improved by 30% by fusing eight or more highly selective stereo pairs, which can achieve an RMSE close to the GSD of the imagery, *i.e.* 4–5 m. As the number of available satellites continues to grow, we expect the temporal, spatial resolution, and the quality of such datasets will further improve, thus facilitating more applications such as global natural disaster monitoring, urban and ecological system monitoring, etc. In future works, we will further evaluate their ability when image/spectral information and 3D information are jointly used for classification and object detection.

Acknowledgements

The authors would like to acknowledge Planet Inc. for providing the Planet images through their research and education program. The LiDAR data are available through the USGS 3D Elevation Program. D. Huang and R. Qin are partially supported by Office of Naval Research (ONR, Award No. N00014-17-1-2928 and N00014-20-1-2141)

Data Availability Statement

The authors will make data/materials supporting the results available upon request, subject to terms and conditions of the source data owners (https://www.planet.com/terms-of-use/).

Declaration

The authors declare no conflict of interest.

Disclosure statement

No potential conflict of interest was reported by the author(s).

Funding

This work was partially supported by Office of Naval Research (ONR, Award No. N00014-17-1-2928 and N00014-20-1-2141).

ORCID

Rongjun Qin http://orcid.org/0000-0002-5896-1379

References

Aati, S., and J.-P. Avouac. 2020. "Optimization of Optical Image Geometric Modeling, Application to Topography Extraction and Topographic Change Measurements Using PlanetScope and SkySat Imagery." *Remote Sensing* 12 (20): 3418. doi:10.3390/rs12203418.

Amitrano, D., G. Di Martino, A. Iodice, F. Mitidieri, M. Nicolina Papa, D. Riccio, and G. Ruello. 2014. "Sentinel-1 for Monitoring Reservoirs: A Performance Analysis." *Remote Sensing* 6 (11): 10676–10693. doi:10.3390/rs61110676.

Bhushan, S., D. Shean, O. Alexandrov, and S. Henderson. 2021. "Automated Digital Elevation Model (DEM) Generation from Very-high-resolution Planet SkySat Triplet Stereo and Video Imagery." *ISPRS Journal of Photogrammetry and Remote Sensing* 173: 151–165. doi:10.1016/j.isprsjprs.2020.12.012.

Breunig, F. M., L. Soares Galvão, R. Dalagnol, C. Eduardo Dauve, A. Parraga, A. Luiz Santi, D. Pinto Della Flora, and S. Chen. 2020. "Delineation of Management Zones in Agricultural Fields Using Cover–crop Biomass Estimates from PlanetScope Data." *International Journal of Applied Earth Observation and Geoinformation* 85: 102004. doi:10.1016/j.jag.2019.102004.

Capaldo, P., M. Crespi, F. Fratarcangeli, A. Nascetti, F. Pieralic, G. Agugiaro, D. Poli, and F. Remondino. 2012. "DSM Generation from Optical and SAR High Resolution Satellite Imagery: Methodology, Problems and Potentialities." Paper presented at the 2012 IEEE International Geoscience and Remote Sensing Symposium, Munich, Germany, 01 July 2012.

Chung, M., Y. Han, and Y. Kim. 2020. "A Framework for Unsupervised Wildfire Damage Assessment Using VHR Satellite Images with PlanetScope Data." *Remote Sensing* 12 (22): 3835. doi:10.3390/rs12223835.

d'Angelo, P., and P. Reinartz. 2021. "Digital Elevation Models from Stereo, Video and Multi-View Imagery Captured by Small Satellites." *ISPRS-International Archives of the Photogrammetry, Remote Sensing and Spatial Information Sciences* 77–82. XLIII-B2-2021. doi:10.5194/isprs-archives-XLIII-B2-2021-77-2021.

Espejo, C., M. M. Jorge, F. Román-Dañobeytia, C. Ascorra, L. Fernandez, and M. Silman. 2018. "Deforestation and Forest Degradation Due to Gold Mining in the Peruvian Amazon: A 34-Year Perspective." *Remote Sensing* 10 (12): 1903. doi:10.3390/rs10121903.

Farr, T. G., P. A. Rosen, E. Caro, R. Crippen, R. Duren, S. Hensley, M. Kobrick, M. Paller, E. Rodriguez, and L. Roth. 2007. "The Shuttle Radar Topography Mission." *Reviews of Geophysics* 45 (2). doi:10.1029/2005RG000183.

Finer, M., S. Novoa, M. J. Weisse, R. Petersen, J. Mascaro, T. Souto, F. Stearns, and R. García Martinez. 2018. "Combating Deforestation: From Satellite to Intervention." *Science* 360 (6395): 1303–1305. doi:10.1126/science.aat1203.

Francini, S., R. E. Mcroberts, F. Giannetti, M. Mencucci, M. Marchetti, G. Scarascia Mugnozza, and G. Chirici. 2020. "Near-real Time Forest Change Detection Using PlanetScope Imagery." *European Journal of Remote Sensing* 53 (1): 233–244. doi:10.1080/22797254.2020.1806734.

Fraser, C. S., and H. B. Hanley. 2003. "Bias Compensation in Rational Functions for IKONOS Satellite Imagery." *Photogrammetric Engineering and Remote Sensing* 69 (1): 53–57. doi:10.14358/PERS.69.1.53.

Ghuffar, S. 2018. "DEM Generation from Multi Satellite PlanetScope Imagery." *Remote Sensing* 10 (9): 1462. doi:10.3390/rs10091462.

Gruen, A., and D. Akca. 2005. "Least Squares 3D Surface and Curve Matching." *ISPRS Journal of Photogrammetry and Remote Sensing* 59 (3): 151–174. doi:10.1016/j.isprsjprs.2005.02.006.

Hirschmuller, H. 2007. "Stereo Processing by Semiglobal Matching and Mutual Information." *IEEE Transactions on Pattern Analysis and Machine Intelligence* 30 (2): 328–341. doi:10.1109/TPAMI.2007.1166.

Kempf, C., J. Tian, F. Kurz, P. D'Angelo, T. Schneider, and P. Reinartz. 2021. "Oblique View Individual Tree Crown Delineation." *International Journal of Applied Earth Observation and Geoinformation* 99: 102314. doi:10.1016/j.jag.2021.102314.

Kim, M., M. Jung, and Y. Kim. 2019. "Histogram Matching of Sentinel-2 Spectral Information to Enhance Planetscope Imagery for Effective Wildfire Damage Assessment." *Korean Journal of Remote Sensing* 35 (4): 517–534.

Kokhan, S., and A. Vostokov. 2020. "Application of Nanosatellites PlanetScope Data to Monitor Crop Growth." *E3S Web of Conferences* 171:02014. doi:10.1051/e3sconf/202017102014.

Loghin, A.-M., J. Otepka-Schremmer, and N. Pfeifer. 2020. "Potential of Pléiades and WorldView-3 Tri-Stereo DSMs to Represent Heights of Small Isolated Objects." *Sensors* 20 (9): 2695. doi:10.3390/s20092695.

Martha, T. R., P. Roy, K. V. K. Nirmala Jain, P. Sashivardhan Reddy, J. Nalini, S. V. S. P. Sharma, K. H. V. D. R. Abhinav Kumar Shukla, and B. Narender. 2021. "Rock Avalanche Induced Flash Flood on 07 February 2021 in Uttarakhand, India—a Photogeological Reconstruction of the Event." *Landslides* 1–13. doi:10.1007/s10346-021-01691-9.

Murakami, H., K. Nakagawa, H. Hasegawa, T. Shibata, and E. Iwanami. 1999. "Change Detection of Buildings Using an Airborne Laser Scanner." *ISPRS Journal of Photogrammetry and Remote Sensing* 54 (2–3): 148–152. doi:10.1016/S0924-2716(99)00006-4.

Podgórski, J., C. Kinnard, M. Pętlicki, and R. Urrutia. 2019. "Performance Assessment of TanDEM-X DEM for Mountain Glacier Elevation Change Detection." *Remote Sensing* 11 (2): 187. doi:10.3390/rs11020187.

Pratima, P., C. M. B. Prakash Chauhan, P. K. Thakur, S. Kannaujia, P. R. Dhote, A. Roy, S. Kumar, S. Chopra, and A. Bhardwaj. 2021. "Cause and Process Mechanism of Rockslide Triggered Flood Event in Rishiganga and Dhauliganga River Valleys, Chamoli, Uttarakhand, India Using Satellite Remote Sensing and in Situ Observations." *Journal of the Indian Society of Remote Sensing* 49 (5): 1011–1024. doi:10.1007/s12524-021-01360-3.

Qin, R. 2014. "Change Detection on LOD 2 Building Models with Very High Resolution Spaceborne Stereo Imagery." *ISPRS Journal of Photogrammetry and Remote Sensing* 96: 179–192. doi:10.1016/j.isprsjprs.2014.07.007.

Qin, R. 2016. "Rpc Stereo Processor (Rsp)–a Software Package for Digital Surface Model and Orthophoto Generation from Satellite Stereo Imagery." *ISPRS Annals of the Photogrammetry, Remote Sensing and Spatial Information Sciences* 77. III-1. doi:10.5194/isprsannals-III-1-77-2016.

Qin, R. 2017. "Automated 3D Recovery from Very High Resolution Multi-view Satellite Images." Paper presented at the ASPRS (IGTF) annual Conference, March 12-16, Baltimore, Maryland, USA.

Qin, R. 2019a. "A Critical Analysis of Satellite Stereo Pairs for Digital Surface Model Generation and A Matching Quality Prediction Model." *ISPRS Journal of Photogrammetry and Remote Sensing* 154: 139–150. doi:10.1016/j.isprsjprs.2019.06.005.

Qin, R. 2019b. "An Operational Pipeline for Generating Digital Surface Models from Multi-Stereo Satellite Images for Remote Sensing Applications." Paper presented at the IGARSS 2019-2019 IEEE International Geoscience and Remote Sensing Symposium, Yokohama, Japan.

Qin, R., J. Tian, and P. Reinartz. 2016. "3D Change Detection–approaches and Applications." *ISPRS Journal of Photogrammetry and Remote Sensing* 122: 41–56. doi:10.1016/j.isprsjprs.2016.09.013.

Reinartz, P., P. d'Angelo, T. Krauß, D. Poli, K. Jacobsen, and G. Buyuksalih. 2010. "Benchmarking and Quality Analysis of DEM Generated from High and Very High Resolution Optical Stereo Satellite Data." *International Archives of the Photogrammetry, Remote Sensing and Spatial Information Sciences:[2010 Canadian Geomatics Conference And Symposium Of Commission I, ISPRS Convergence In Geomatics-Shaping Canada's Competitive Landscape] 38 (2010),* Calgary, Alberta, Canada, *Nr. Part 1* 38 (Part 1). doi: 10.15488/1121.

Sagan, V., M. Maimaitijiang, S. Bhadra, M. Maimaitiyiming, D. R. Brown, P. Sidike, and F. B. Fritschi. 2021. "Field-scale Crop Yield Prediction Using Multi-temporal WorldView-3 and

PlanetScope Satellite Data and Deep Learning." *ISPRS Journal of Photogrammetry and Remote Sensing* 174: 265–281. doi:10.1016/j.isprsjprs.2021.02.008.

Shi, H., S. Yang, and G. Liu. 2011. "The Application of InSAR in the Deformation Monitoring for Road engineering-A Case Study: Dujiangyan, China." Paper presented at the 2011 Fourth International Conference on Intelligent Computation Technology and Automation, Shenzhen, China.

Shugar, D. H., M. Jacquemart, D. Shean, S. Bhushan, K. Upadhyay, A. Sattar, W. Schwanghart, S. McBride, M. Van Wyk de Vries, and M. Mergili. 2021. "A Massive Rock and Ice Avalanche Caused the 2021 Disaster at Chamoli, Indian Himalaya." *Science* 373 (6552): 300–306. doi:10.1126/science.abh4455.

Stal, C., F. Tack, P. De Maeyer, A. De Wulf, and R. Goossens. 2013. "Airborne Photogrammetry and Lidar for DSM Extraction and 3D Change Detection over an Urban Area–a Comparative Study." *International Journal of Remote Sensing* 34 (4): 1087–1110. doi:10.1080/01431161.2012.717183.

Team, P. "Planet Application Program Interface: In Space for Life on Earth." https://api.planet.com

Tian, J., P. Reinartz, P. d'Angelo, and M. Ehlers. 2013. "Region-based Automatic Building and Forest Change Detection on Cartosat-1 Stereo Imagery." *ISPRS Journal of Photogrammetry and Remote Sensing* 79: 226–239. doi:10.1016/j.isprsjprs.2013.02.017.

Wang, S., Z. Ren, W. Chuanyong, Q. Lei, W. Gong, Q. Ou, H. Zhang, G. Ren, and L. Chuanyou. 2019. "DEM Generation from Worldview-2 Stereo Imagery and Vertical Accuracy Assessment for Its Application in Active Tectonics." *Geomorphology* 336: 107–118. doi:10.1016/j.geomorph.2019.03.016.

Wright, T. J., B. E. Parsons, and L. Zhong. 2004. "Toward Mapping Surface Deformation in Three Dimensions Using InSAR." *Geophysical Research Letters* 31 (1). doi:10.1029/2003GL018827.

Xiaowei, Y., J. Hyyppä, A. Kukko, M. Maltamo, and H. Kaartinen. 2006. "Change Detection Techniques for Canopy Height Growth Measurements Using Airborne Laser Scanner Data." *Photogrammetric Engineering and Remote Sensing* 72 (12): 1339–1348. doi:10.14358/PERS.72.12.1339.